Supplementary Appendix

Polyclonal Cryptal Genesis and Development of Familial Small Intestinal Neuroendocrine Tumors

Yoshitatsu Sei, Jianying Feng, Xilin Zhao et al.

Table of Contents

I. Supplementary Methods

Expression of mRNA by RNA-ISH

Human jejuno-ileal tissue and SI-NET samples were formalin fixed, embedded in paraffin, and cut into 5 μm sections. Expression of mRNA on the formalin fixed paraffin-embedded sections were examined by *in situ* hybridization system (QuantiGene View RNA ISH tissue assay, Affymetrix, Santa Clara, CA) with probes specific to the genes of our interest according to the manufacturer's instruction. The probes used in this studies were TPH1 (VA6-12882-01 or VA1-13091-06), DCLK1 (VA1-1401-06), TAC1 (VA6-15836-01), NTS (VA1-15621-01), CCK (VA1-15617-01), SST (VA1-10301-06), GCG (VA6-11294-06), GHRL (VA6-15619-01), GIP (VA6-15620-01), SCT (VA6-15618-01), PCGF4 (VA1-13756-01), HOPX (VA1-12410-06), SOX9 (VA1-10452-06), NEUROD1 (VA6-13884-01), CHGA (VA6-13875-01), Lrig1 (VA6-12609-06), LGR5 (VA6-12588-06), and NEUROG3 (VA6-13489-02). RNA-ISH signals were detected by the chromogens fast red and fast blue. After the hybridization, the tissue sections were counterstained with Gill's hematoxylin and then stained with DAPI. The chromogens were examined using both bright field and fluorescence microscopy. For the examination of fluorescent signals, fast red and fast blue fluorescent signals were examined with excitation/emission wave-length 530/590 nm and 630/775 nm, respectively, using Zeiss LSM510 Meta confocal microscope (Carl Zeiss, USA). For the image analysis, the images of fast red fluorescence (pseudo-colored in red) and fast blue fluorescence (pseudo-colored in green) were merged with transmitted light image using the LSM510 Meta software to visualize the locations of the cells and the expressions of the mRNAs simultaneously.

Cytochrome c oxidase histochemistry followed by immunohistochemistry

Human jejuno-ileal tissue and SI-NET samples were embedded within Tissue-Tek OCT, frozen on dry ice and kept in a –80°C freezer until sectioning. Frozen sections were made at a 10 μm thickness on a cryostat. A dual-color histochemical enzyme assay was performed to determine mtDNA-encoded cytochrome c oxidase (CCO) and nuclear DNA-encoded succinate dehydrogenase (SDH) according to the method previously described [1]. Briefly, frozen sections were first incubated in cytochrome *c* oxidase medium (100 mM cytochrome c, 4 mM diaminobenzidine tetrahydrochloride, and 20 mg/ml catalase in 0.2 M phosphate buffer, pH 7.0) at 37°C for 50 minutes. Sections were washed in PBS three times for 5 minutes per wash. The sections were then incubated in SDH medium (130 mM sodium succinate, 200 mM phenazine methosulphate, 1 mM sodium azide, 1.5 mM nitroblue tetrazolium in 0.2 M phosphate buffer, pH 7.0) at 37°C for 40 minutes. Sections were washed in PBS three times for 5 minutes per wash, dehydrated in a graded ethanol series (2x70%, 2x95% and 2×100%, 2 minutes per each incubation), and air-dried for 5 minutes. To proceed with immunohistochemistry, the sections were fixed with cold acetone for 10 minutes at -20°C. The sections were incubated in PBS containing 10% non-immune goat serum for 10 minutes at RT and then immunostained with 1:800 mouse monoclonal anti-chromogranin A (LK2H10, #MS-324-P, Thermo Scientific, Cheshire, UK) at RT for one hour in PBS containing 5% fetal bovine serum. After incubation with primary antibody, the sections were incubated with 1:1000 Alexa Fluor 594-conjugated goat anti-mouse IgG secondary antibody (Invitrogen, Carlesbad, CA) for 30 min at RT and with DAPI for 1 min at RT. The sections were observed, imaged and analyzed using a Zeiss LSM510 Meta confocal

microscope (Carl Zeiss USA).

Crypt preparation and immunohistochemistry

Human jejuno-ileal tissue and SI-NET samples were either immediately processed for the experiment or cryopreserved in Cryoscarless DMSO-free solution (BioVerde Inc, Japan) and stored in liquid nitrogen until analysis. The cryopreserved tissues were thawed, transferred into cold DMEM and cut into small pieces. Crypt-enriched preparations were obtained by incubation in DPBS containing 2mM EDTA for 30 min at 4^{o}C followed by vigorous pipetting. The crypt-enriched materials were fixed in 4% paraformaldehyde in DPBS for one hour at room temperature and treated with DPBS containing 0.1% triton X-100 for 30 min. Crypts were incubated in DPBS containing 5% fetal bovine serum for 1 hr at RT and then immunostained with 1:500 mouse monoclonal anti-chromogranin A (LK2H10) (#MS-324-P, Thermo Scientific, Cheshire, UK) at RT for one hour in DPBS containing 5% fetal bovine serum. After incubation with primary antibody, crypt-enriched samples were incubated with either Alexa Fluor 488 or 647 -conjugated goat anti-mouse IgG secondary antibody (highly cross-adsorbed, Invitrogen, Carlesbad, CA) for 30 min at RT and with DAPI for 1 min at RT. For double staining with anti-Bmi1 antibody, following a complete Alexa Fluor 488-ChgA immunostaining, crypt-enriched preparations were incubated with anti-Bmi1 antibody (1:50, IHC-00606, Bethyl, Montgomery, TX) at 4C overnight in DPBS containing 5% fetal bovine serum. The crypt-enriched preparations were then incubated with Alexa Fluor 647 -conjugated goat anti-rabbit IgG antibody for 30 min at RT and with DAPI for 1 min at RT. Immunostained cyrpts were observed, imaged and analyzed using Zeiss LSM510 Meta confocal microscope (Carl Zeiss USA).

Sequencing of mitochondrial DNA (mtDNA)

DNA was isolated using QIAamp DNA FFPE tissue kit or DNA micro kit from isolated crypts or laser micro-dissected tissues, respectively. A portion of mtDNA that covers Complex IV gene region was sequenced using the method described by Ramos et al [2]. PCR products were purified using QIAquick PCR purification kit and Sanger sequenced.

II. Supplementary Result and Discussion

Human EC cells co-express TPH1 and Tac1 both in the crypt and villus of ileal mucosa.

Tryptophan hydroxylase 1 (TPH1) is primarily expressed in EC cells of the gastrointestinal tract and catalyzes biosynthesis of serotonin (5-hydroxytryptamine, 5HT) [3]. To establish the basis for an endocrine gene expression profile of EC cells for this study, we examined the co-expression of mRNA coding for various endocrine peptides in TPH1 mRNA-expressing cells using two-color RNA in situ hybridization (RNA-ISH). In human ileal mucosa, TPH1-expressing cells were abundant and co-expressed substance P precursor gene tachykinin 1 (Tac1) mRNA. Tac1 was always expressed in the TPH1-positive cells regardless of their location (Supplementary Figure S3 A and D). TPH1-expressing cells did not co-express proglucagon (GCG, glucagon-like peptide 1, GLP1) and neurotensin (NTS) (Supplementary Figure S3 B and E) nor gastric inhibitory polypeptide 1 (GIP1) and somatostatin (SST) (data not shown). Enteroendocrine cells expressing secretin (SCT), ghrelin (GHRL) or cholecystokinin (CCK) were rare to absent in ileal tissue (data not shown).

In summary, the current RNA-ISH studies showed that TPH1 positive EC cells in the ileal mucosa selectively co-express the Tac1 gene encoding substance P and neurokinins without expression of other enteroendocrine cell genes such as GCG, CCK, GIP, SCT, NTS, GHRL, or SST (see Supplementary Result section). This is consistent with a revised enteroendocrine cell type model by Engelstoft et al. which proposes that 5HT secreting EC cells belong to a substance P expressing group of enteroendocrine cells that mediates GI motility and metabolism and differs from the group of enteroendocrine cells expressing various combinations of six functionally related peptide hormones CCK, GIP, GLP-1, PYY, NTS and SCT that mediate satiety-related functions [4]. TPH1 positive EC cells all expressed the basic helix-loop-helix transcription factor NeuroD1 necessary for enteroendocrine differention in the GI tract and neuroendocrine secretory marker protein ChgA regardless of their positions within the crypt-villus axis. Since the SI-NETs examined in this study were positive for TPH1, Tac1, NeuroD1 and ChgA and negative for GCG or NTS, the results support the generally accepted proposal that the SI-NET originates from a group of 5HT and substance P producing EC cells [5-8].

Mathematical analysis of expected mutant cell-derived intestinal patch size.

In the human ileum, the density of crypts is approximately 5,000 crypts/cm^2 [9, 10]. The area of a circle of radius R cm contains *N* crypts = π x R^2 x 5,000. The number of crypt replication cycles needed to produce *N* crypts is $\log_2 N$. An estimated normal crypt replication cycle is from 9 years to more than 30 years [11-13]. In patient F10, the shortest distance between two tumors is 7.5 cm (Figure 5). If the two tumors shared the same mutant cell origin, the minimal patch size would have a radius of 7.5 cm encompassing 880,000 crypts. This would require a minimum of 19.8 crypt cycles spanning a minimum of 178 years assuming a normal crypt replication cycle. Therefore, it is unlikely that the two tumors in 48 yo patient F10 were derived from the patch originating from the same mutant cell.

However, an accelerated crypt cycle associated with pathological conditions has been reported [14]. No underlying pathological conditions such as ulcerative colitis or Crohn's disease was present in this patient. Nonetheless, we examined the crypt branching process in the tumor tissue sections to estimate the crypt replication cycle using the method established by Cheng et al [14]. Using this method, the duration of the crypt replication cycle Tr can be calculated by the following equation [14]:

$$Tr = Tb \times \ln 2 / \ln(1+Ib)$$

Where Tb is the duration of the branching process and Ib is the fraction of branching crypts in the epithelium. Since stem cells in the distal small intestine divide only 2/3 as frequently as those in the large intestine [10] and Tb=20-40 days for the large intestine [14], Tb for the distal human small intestine is roughly 30-60 days. Interestingly, the observed average fraction of the crypt branching process near or within the two tumors was 1.75% (n=6, n=3 per each tumor), which was higher than the normal range of 0.44%. Thus, Tr=Tbxln2/ln1.0175=(30 to 60) x40.1=1203 to 2406 days=3.3 to 6.6 years. Therefore the crypt replication cycle in the tumor areas of the patient was mildly more accelerated than the normal crypt cycle (9-30 years). However, even at this accelerated rate, the completion

of 19.8 crypt cycles would be expected to span an unlikelly period of 65-130 years for this 45 yo patient. Moreover, this estimate is based on the observed average crypt branching process near or within two tumors. Although the fraction of the crypt branching process in the area between the tumors is not available, it is likely to be closer to the normal range (0.44%). Therefore we expect that the estimated duration to establish a single mutant cell-derived patch spanning over the area of a circle of radius 7.5 cm would be longer than 65-130 years.

In conclusion, although a mildly accelerated crypt replication cycle near and within the tumors was observed (which may have some important implications for tumorigenesis), a single mutant cell-derived patch spanning over the area of a circle of radius 7.5 cm is unlikely in a 45 yo patient F10.

III. Supplementary Figures

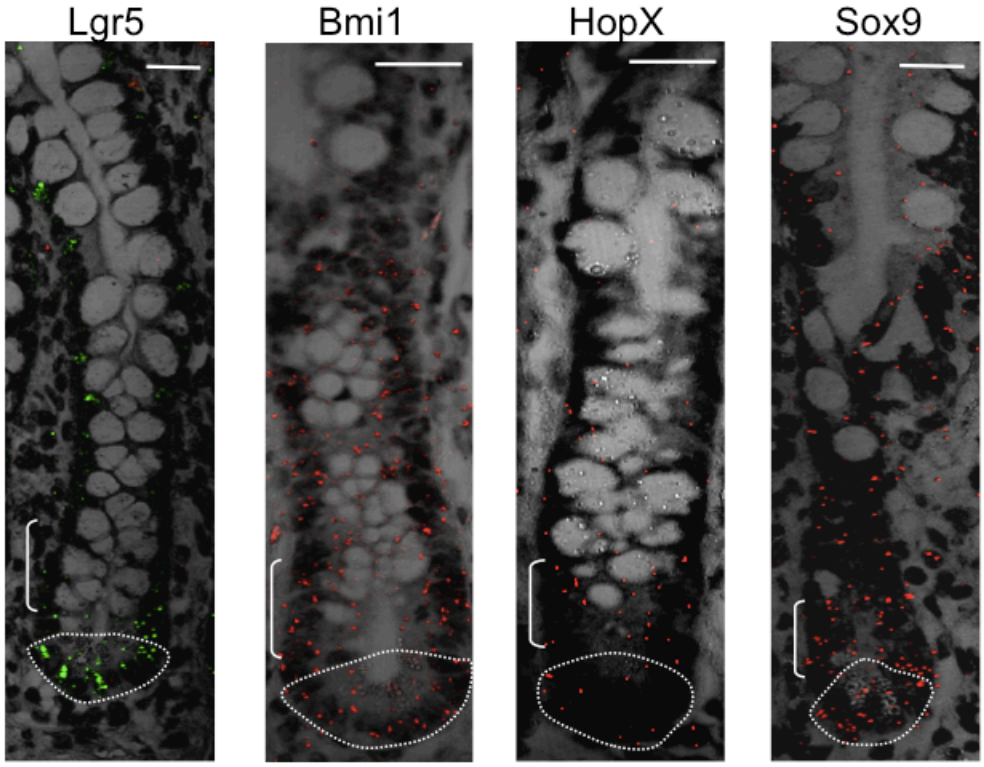

Supplementary Figure S1. Expression of Lgr5, Bmi1, HopX and Sox9 in human ileal crypt cells. The RNA-ISH images for Bmi1, HopX and Sox9 (fast red fluorescence, red) or Lgr5 (fast blue fluorescence, green) expression were merged with transmitted light images from human ileal FFPE sections to visualize their pattern of expression. The white dotted lines indicate the crypt bottom region and the solid lines indicate the area between position 5 and 10. Scale bars, 20 μm. Representative RNA-ISH image for Sox9 was from patient F2 and the other images from patient F1.

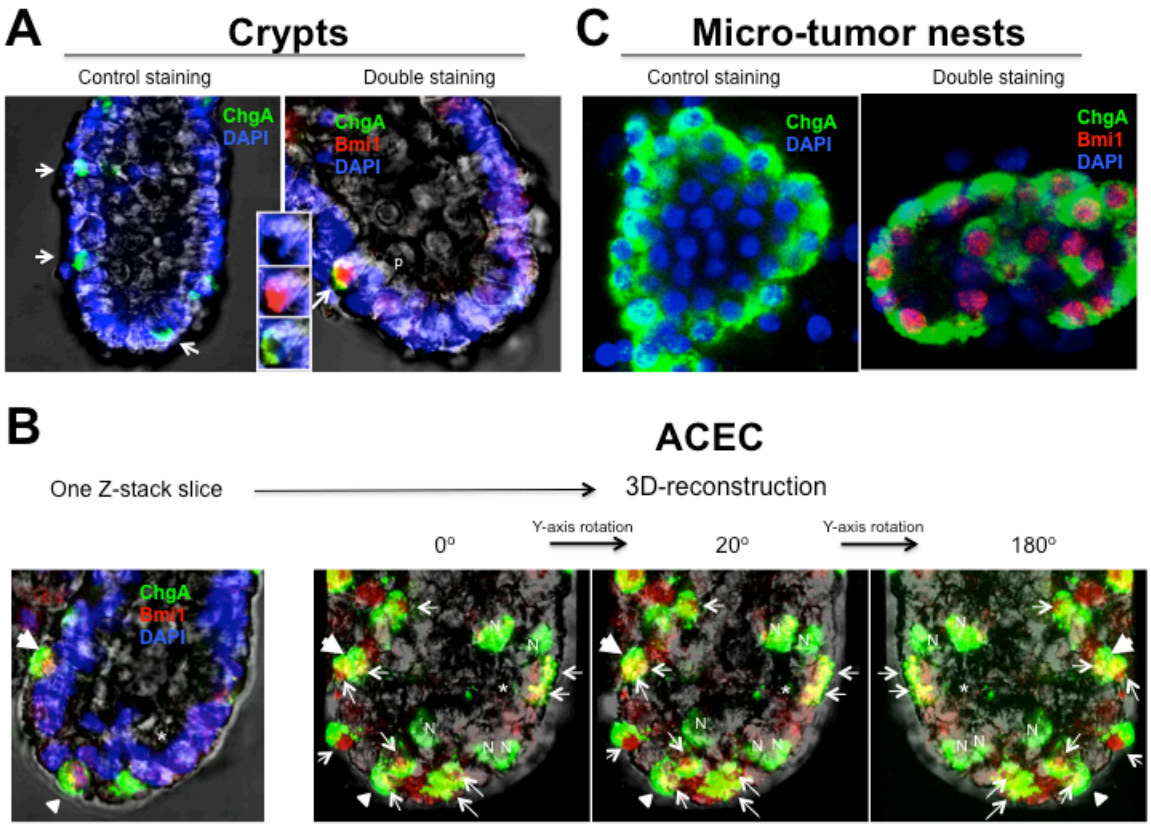

Supplementary Figure S2. Immunohistochemical detection and characterization of Bmi1+ ChgA+ cells in the normal crypts, ACEC and micro-tumor nests in the ileal crypt preparation from a patient with familial SI-NET (F13). (**A**) Representative images of IHC of isolated crypts merging fluorescent and transmitted light images to visualize cell location and immunoreactivities. A crypt in the contnrol left panel was stained without α-Bmi1 rabbit antibody (Ab), but with the secondary Alexa 647-α-rabbit Ab following immunostaining with α-ChgA mouse monoclonal Ab /Alexa 488-α-mouse Ab. The arrows point to ChgA+ enteroendocrine cells (green) that were negative for the Alexa 647 fluorescence, indicating no cross-reactivity between Abs. A crypt in the right panel was double stained with α-Bmi1 and α-ChgA Ab. The highest Bmi1 immunoreactivity was found in a ChgA+ cell at position 4 (arrow). An inset (from top to bottom) shows DAPI (blue), ChgA (green) and Bmi1 (red) images of the +4 cell (arrow), respectively. ChgA immunoreactivity is mainly cytoplasmic whereas Bmi1 is nuclear. P indicates a position of the highest Paneth cell seen in this crypt. (**B**) Representative IHC images of early stages of ACEC containing multiple Bmi1+ ChgA+ double positive cells. One of the Z-stack confocal sections (left) indicates two Bmi1+ ChgA+ double positive cells at position 4 (arrowhead) and crypt base (triangle) in an early ACEC. Analysis of 3D images reconstructed from the Z-stack confocal images of the ACEC shows a total of 15 ChgA+ cells in the crypt (10 ChgA+ cells are below position +4). A Paneth cell (*), two Bmi1+ ChgA+ double positive cells at position 4 (arrowhead) and crypt base (triangle) seen in a Z-stack section (left) were

marked in these 3D images. Rotation of these images indicates that two thirds of ChgA+ cells (arrows) are Bmi1 positive. N indicates Bmi1 weak or negative ChgA+ cells. (**C**) Representative IHC images of micro-tumor nests. A micro-tumor (left panel) was stained without α-Bmi1 Ab, but with the Alexa 647 secondary Ab following ChgA immunostaining. The tumor cells in the nest are all ChgA positive without any cross-reactivity with the Alexa 647 secondary Ab. Because of cellular polarization of inward oriented apical surfaces, outward ChgA immunoreactive cytoplasm of the cells in the center area is invisible in this confocal section. A micro-tumor (right panel) was double stained with α-Bmi1 and α-ChgA Ab. The majority of cells in this micro-tumor show cytoplasmic ChgA and nuclear Bmi1 immunoreactivity.

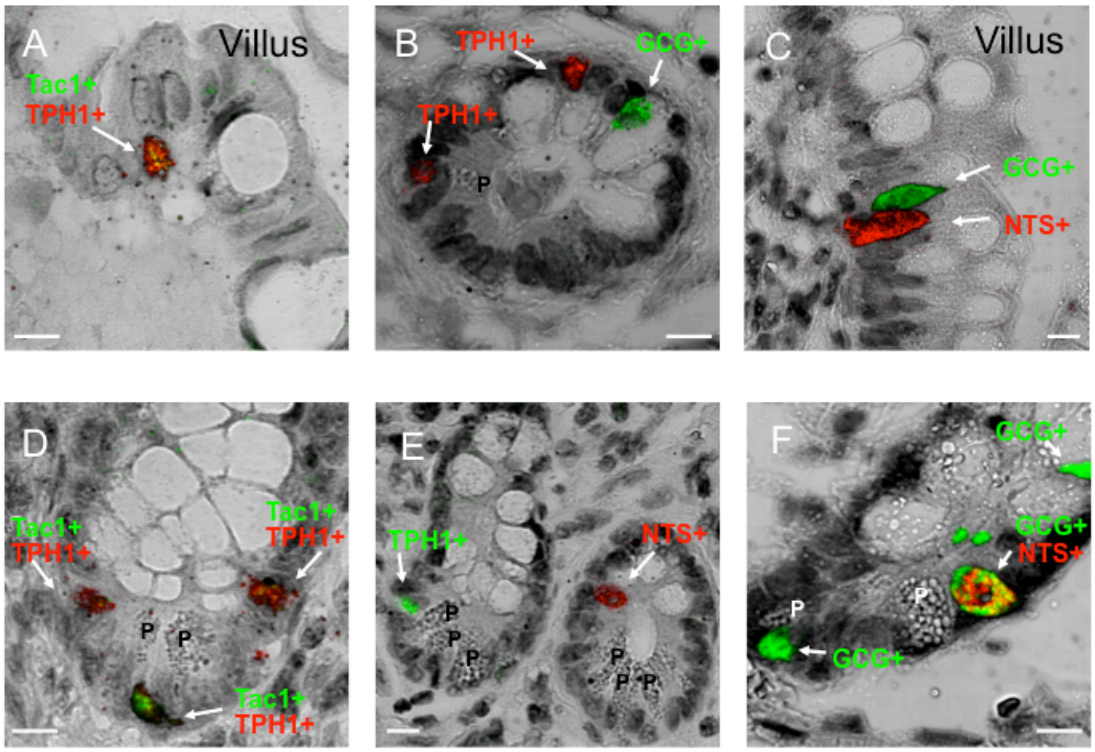

Supplementary Figure S3. Expression of endocrine hormone genes in human ileal EC cells. RNA-ISH images of TPH1 (red in A, B and D, or green in E) and indicated secretory hormone gene expression (Tac1 and GCG, green and NTS, red) were merged with transmitted light images to visualize the identity and location of enteroendocrine cells within the crypt and villus. (**A**) Tac1 expression in a TPH1+ EC cell in the villus. (**B**) Two TPH1+ EC cells and a separate GCG+ enteroendocrine cells in the crypt without gene co-expression. (**C**) GCG+ and NTS+ enteroendocrine cell side by side in the villus without co-expression of the two genes. (**D**) Three Tac1+/TPH1+ EC cells in the crypt. The EC cell at the crypt base showed high Tac1 and low TPH1 expression. (**E**) NTS+ and TPH1+ EC cells appear in separate crypts in the same field with absence of co-expression of the two genes. (**F**) Co-expressing NTS+/GCG+ enteroendocrine cells were seen at position 4. NTS-/GCG+ cells were seen at the crypt base and position 9. The frequency of doubly positive GCG+ /NTS+ cells was approximately 50% in the cells located below position 4 and diminished to 7% in the cells located above position 11. This decreasing gradient pattern of hormone co-expression along the crypt-villus axis was similar to our previous findings in the duodenum of CCK-GFP transgenic mice where co-expression of CCK, ghrelin and GIP was frequent in cells below +4 position and rare in higher positions [15]. In contrast, Tac1 was always expressed in the TPH1-positive cells regardless of their location in the crypt and the villus. P indicates Paneth cell. Scale bars: A-F, 10 μm. Representative RNA-ISH images were from control patient, C1.

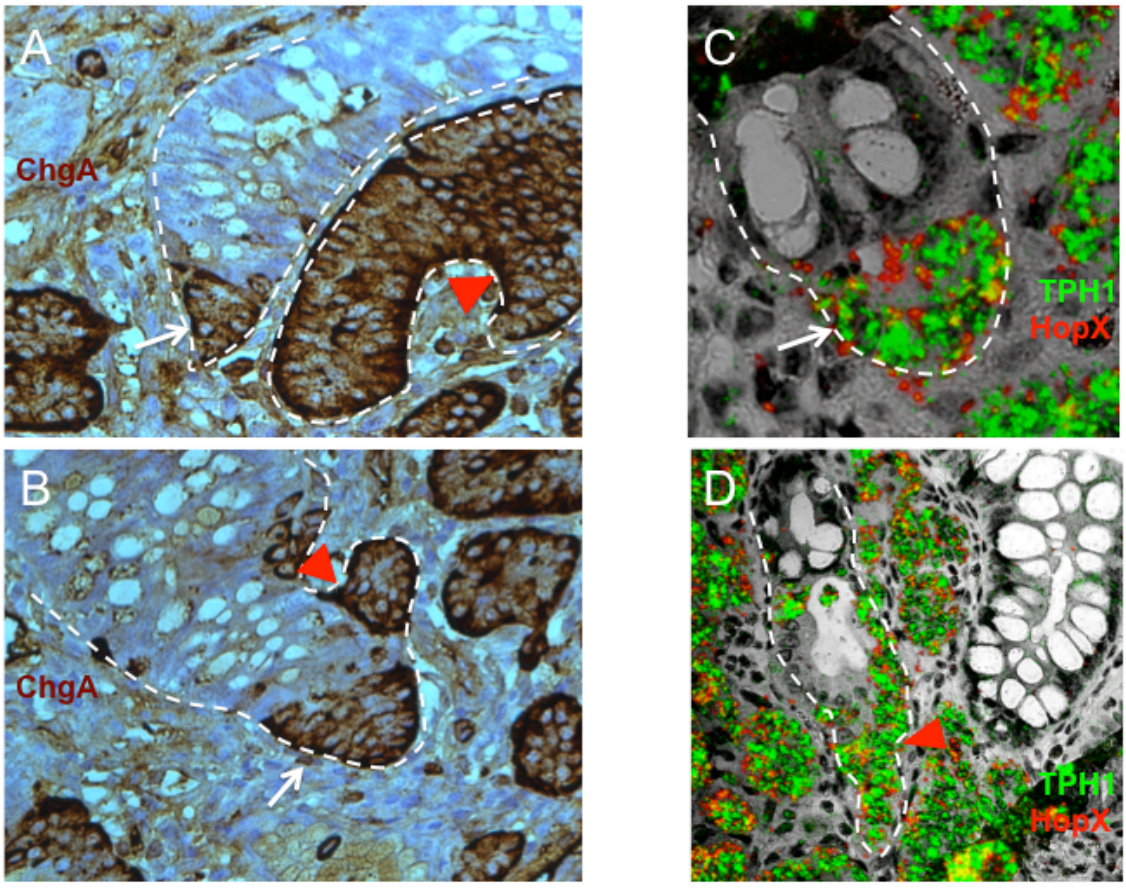

Supplementary Figure S4. Examples of ACECs and budding of ACECs in the ileal tissues from patients F12 (A and B) and F11 (C and D). (**A**) Tissue section immunostained for ChgA showed an early (white arrow, left) ACEC and an advanced ACEC (right). Arrowhead marks putative area of budding. (**B**) Another early ACEC, which was accompanied by budding (arrowhead), was evident in the ChgA-immunostained section. (**C and D**) RNA-ISH showed an early ACEC (C) and an advanced ACEC (D). *TPH1* (green) and *HopX* (red) were highly expressed in both ACECs and in neighboring extraepithelial tumor nests. Arrowhead marks putative area of budding. We define "budding of ACEC" as an obvious indentation of the epithelium of the ACEC as a result of new asymmetric growth in the epithelium. We suggest this process is central to the genesis of micro-tumors projecting into the surrounding submucosa. We hypothesize that extra-epithelial tumor islands or nests are generated from pinching off of buds from ACECs.

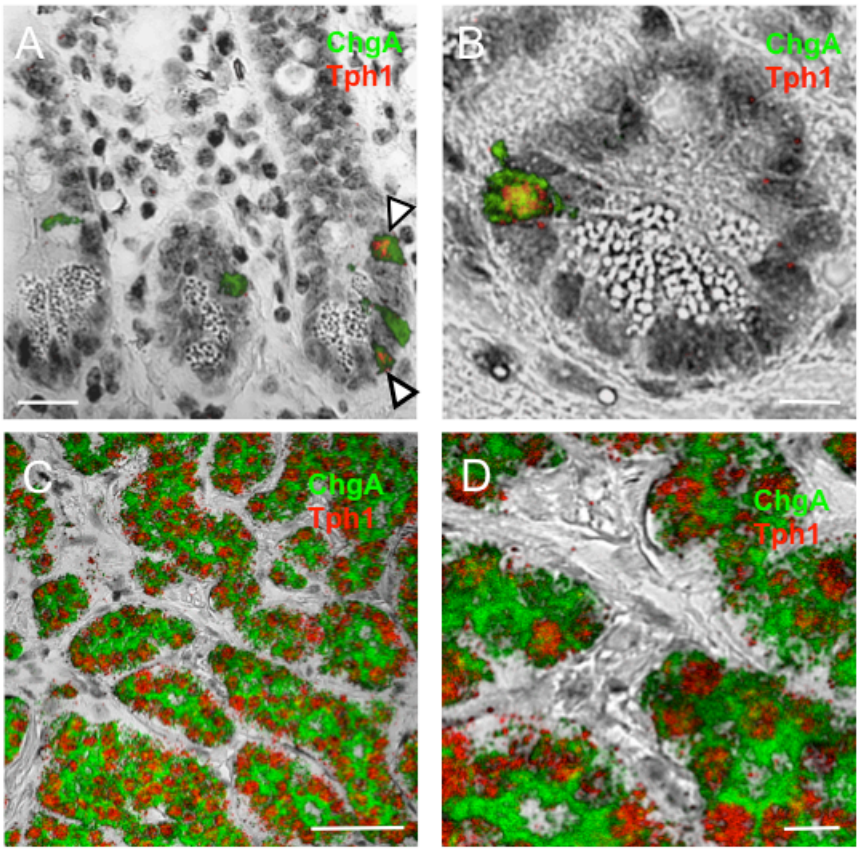

Supplementary Figure S5. Expression of ChgA and TPH1 in human ileal epithelium and SI-NET cells. The RNA-ISH images for expression of TPH1 (fast red fluorescence, red) and ChgA (fast blue fluorescence, green) were merged with transmitted light images. (**A**) Two ChgA+/TPH1+ EC cells (triangles) and three ChgA+/TPH1- cells (non-EC enteroendocrine cells) were detected. (**B**) Detection of a ChgA+TPH1+ EC cell at position 4. (**C** and **D**) High co-expression of ChgA and TPH1 in SI-NET cells. ChgA was highly localized in the cytoplasm while TPH1 was predominantly within the nucleus. Scale bars in A, 20 μm; in B and D, 10 μm; in C, 50 μm. Representative RNA-ISH images were from patient F4.

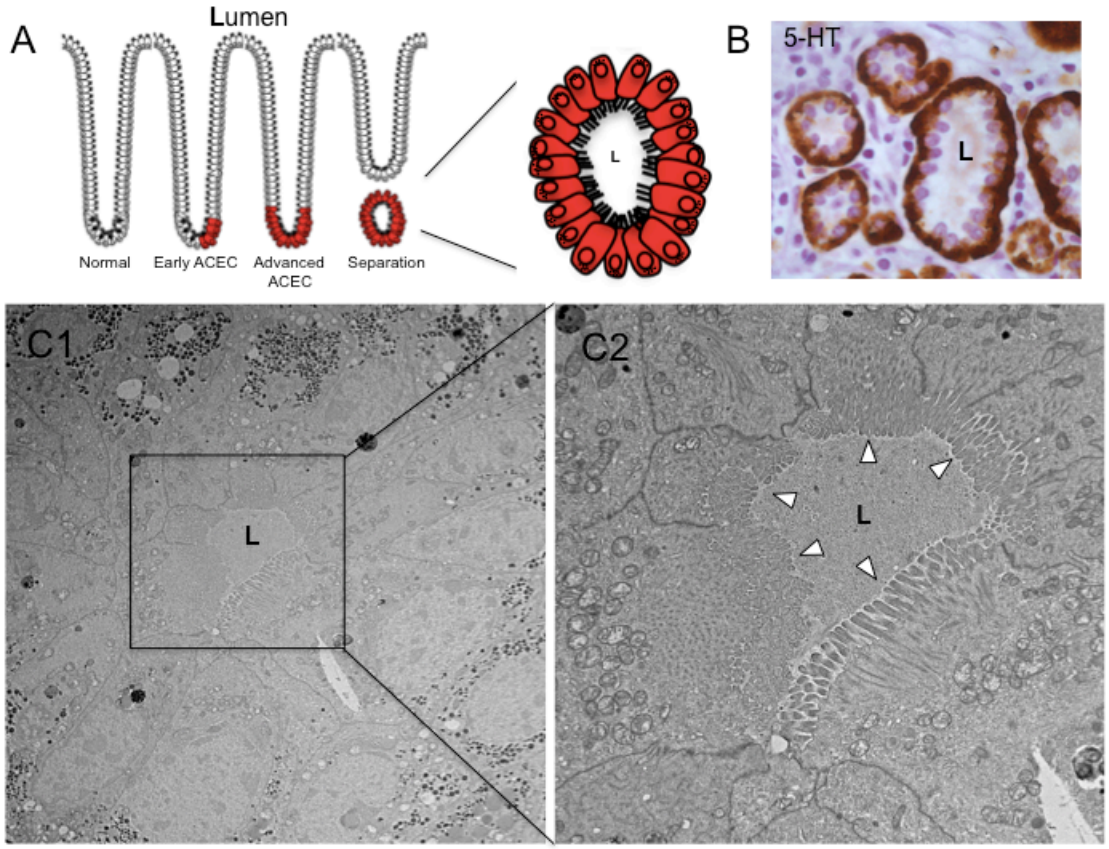

Supplementary Figure S6. Histological and electron micrographic support for the crypt based hypothesis of SI-NET tumorigenesis . (**A**) Cartoon model of the hypothetical formation and development of an epithelial based ACEC leading to the origin of an extra-epithelial tumor nest upon separation from the epithelial layer. L=Luminal side. (**B**) Immunohistochemical detection of 5HT in an FFPE section of a SI-NET shows positive tumor nests with luminal centers reminiscent of a crypt-like architecture with cellular polarization of inward oriented apical surfaces and basal 5HT staining (**C**) Electron micrographs of a SI-NET nest. **C1**; A low magnification electron micrograph of a small tumor nest similar to nests in panel B shows a central lumen (L) and peripheral basal dense secretary granules. **C2**; Higher magnification electron micrograph of the inset from panel C1 shows the presence of luminal facing microvilli (arrow heads) and supports the concept of some extra-epithelial (probably early) tumor nests taking on an ordered structure with features of their cryptal origin.

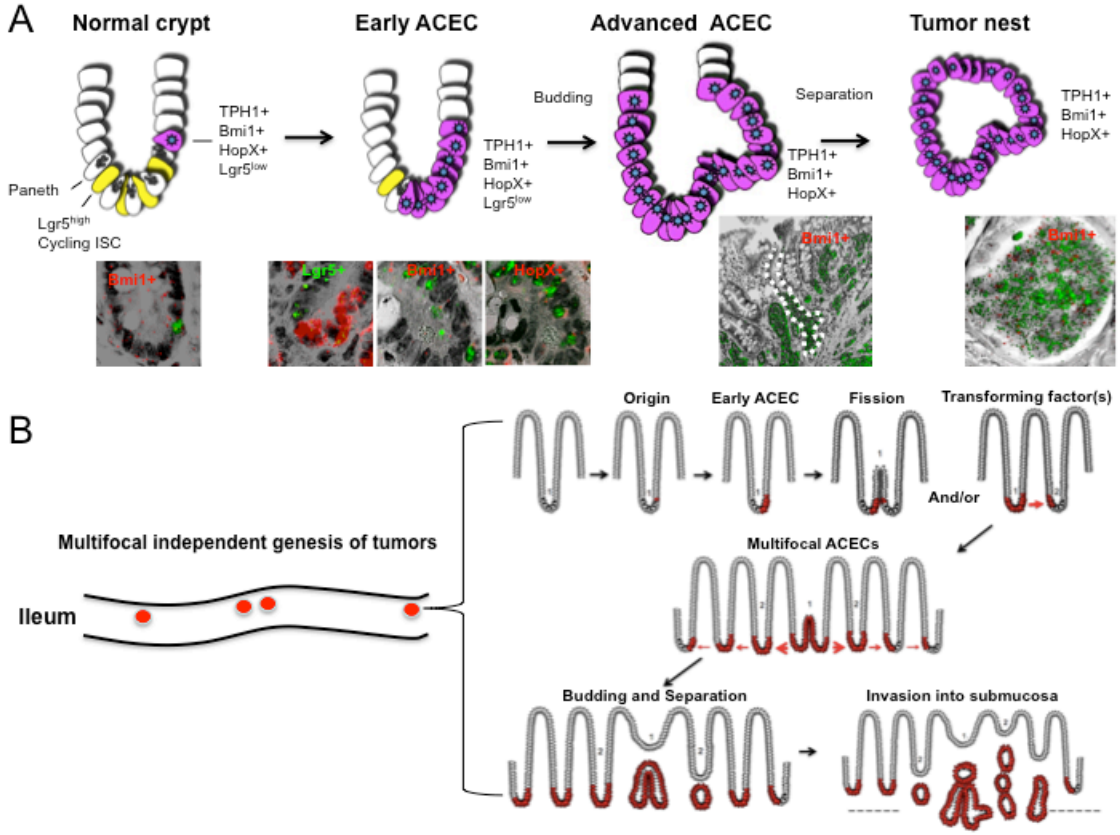

Supplementary Figure S7. Evidenced based model for the multifocal and polyclonal genesis of reserve ISC gene-expressing cryptal tumors and their development in patients with Familial SI-NET carcinoid. (**A**) Hypothetical multifocal and polyclonal genesis of the SI-NETs and their growth was modeled from the results of the current study and previously reported studies. SI-NETs are proposed to originate from +4 EC cells expressing reserve ISC genes, Bmi1, HopX and Lgr5^{low} (colored in Purple). The early tumor formation starts at the crypt bottom to form an ACEC (TPH1+, Bmi1+, HopX+ and Lgr5^{low}) and undergoes "bottom-up" morphogenesis. Advanced ACECs produce buds that become extra-epithelial tumor nests following separation from the epithelial layer. Extra-epithelial tumor nests express TPH1+, Bmi1+, HopX+ as well as other reserve ISC genes Lrig1 and DCLK1, but tend to lose Lgr5 expression. Representative images are from Figure 1, 3A-right, 4A-center, 4A-right, 4B and 2A, respectively. (**B**) Cartoon model for the proposed genesis and development of an independent multifocal tumor in patients with familial SI-NETs by the multifocal and polyclonal genesis of ACECs. The initial progenitor (presumably +4 EC-reserve ISC) advances to an ACEC within an individual crypt. The transformed crypt spreads to generate other transformed crypts by fission and/or transformation of neighboring crypts by a local field effect. Through these processes, a nascent tumor comprised of multifocal ACECs advances by budding and subsequent separation of the advanced ACECs from the epithelial layer (see supplementary Figure S5) to create extra-epithelial tumor nests that invade into the submucosa and ultimately the muscle and serosa. The data shown in Figures 5, 6 and 7 suggest that this proposed model of

tumorigenesis occurs independently at multiple sites, resulting in the multifocal synchronous tumors observed in patients with familial SI-NET.

IV. Supplementary Tables

Supplementary Table 1

Patient#	Age	Sex	Primary Site	Bowel Tumors (#)	Lymph Nodes (#)	Primary Size (mm)	TNM Class	Stage	Grade
F1	58	M	I	29	4	11	T2N1M0	IIIB	G1
F2	57	M	J	7	1	7	T4N1M0	IIIB	G1
F3	45	F	I	34	2	1.3	T2N1M0	IIIB	G1
F4	60	M	I	5	0	5	T2N0M0	IIA	G1
F5	65	M	J-I	2	0	6	T1N0M0	I	G1
F6	56	M	I	4	0	8	T1N0M0	I	G1
F7	83	M	I	2	ND	3.5	T4N1M1	IV	G1
F8	53	F	J	1	ND	ND	T4N1M0	IIIB	G1
F9	47	M	ND	9	0	2.5	T4N1M1	IV	G1
F10	85	M	ND	7	0	10	T4N0M0	IIIA	G1
F11	57	F	I	2	4	13	T4N1M1	IV	G1
F12	52	F	I	10	15	25	T4N1M0	IIIB	G1
F13	45	M	I	136	23	1.5	T4N1M0	IIIB	G1
F14	68	M	I	1	0	8	T2N0M0	IIA	G1
S1	28	M	I	1	5	8	T4N1M1	IV	G1
C1	64	M	NA	NA	NA	NA	NA	NA	NA

F1-F14; patients with familial SI-NET, S1; a patient with sporadic SI-NET, C1; a control patient without SI-NET
F2, F4 and F5 are affected patients from the family who was linked to IPMK.
F7 and F14 are also relared. The rest of nine patients with familial SI-NET (Fs) are unrelated.

Supplementary Table 2

The gene expression status in the SI-NET

Patient	Tissue	Expression status of the genes tested by RNA in situ										
		RC stem	Reserve stem				Pan stem	Enteroendocrine				
#		Lgr5	Bmi1	DCLK1	HopX	Lrig1	Sox9	Ngn3	NeuroD1	EC cell TAC1	EC cell TPH1	ChgA#
F1	Ileum	N	p	p	p	P	N	N	P	p	p	
F2	Ileum	N**	P		P		N*	N	P		P	
F3	Ileum	N	P	P	P	P	Pw	N	P		P	
F4	Ileum	N	P				N	N	P		P	P
F5	Ileum	N		P	P	P			P	p	p	
F6	Ileum	N		P	P	P					p	
F7	Liver	N	P	P	P	P		N			P	
F8	Ileum	N*	P	P	P	P					P	
F9	Liver	N	P	P	P	Pw					P	
F10	Ileum	P	P	P	P	P					P	P
F11	Ileum	N	P	Pw	P	P					P	P
F12	Ileum	N	P	Pw	P	P					P	P
F13	Ileum											
F14	Ileum											
S1	Ileum	N	P	Pw	P	P					P	
C1	Ileum											

F1-F14; patients with familial SI-NET, S1; a patient with sporadic SI-NET, C1; a control patient without SI-NET
*P=positive, N=negative, w=weak, *only a countable positive cells were found in a few tumor nests in this patient*
*** All the tumor nests were negative for Lgr5 except the early ACEC shown in Figure 3A*
#, all the tumor samples were routinely tested for ChgA immunoreactivity and tested all positive.
A blank means "not tested".

Supplementary Table 3

Patient #	Tissue	Patients examined for the study (Table#s or Fig#s)				Presence of ACECs in the examined materials	
		Normal TPH1+ cells RNA in situ study	Tumor cells RNA in situ study	mt-DNA CCO- study		ACECs	ACECs with Budding
F1	*Ileum*	Fig1	Table 2, Fig2				
F2	*Ileum*	Fig1	Table 2, Fig 2			Figs 3,4*	Fig 4
F3	*Ileum*		Table 2				
F4	*Ileum*	Fig1	Table 2, Fig S4				
F5	*Ileum*		Table 2, Fig 2				
F6	*Ileum*		Table 2				
F7	*Liver*		Table 2				
F8	*Ileum*		Table 2				
F9	*Liver*		Table 2				
F10	*Ileum*		Table 2			Fig 5*	
F11	*Ileum*		Table 2, FigS4			Fig S4*	Fig S4
F12	*Ileum*		Table 2			Fig S4	Fig S4
F13	*Ileum*			Fig 6		Fig 6	**
F14	*Ileum*			Fig 7		Fig 7	
S1	*Ileum*		Table 2				
C1	*Ileum*	Fig1, Fig S3					

F1-F14; patients with familial SI-NET, S1; a patient with sporadic SI-NET, C1; a control patient without SI-NET
* Expressions of Bmi1 and/or HopX were shown by RNA-ISH.
** Found in 4% paraformaldehyde-fixed crypt preparation after ChgA immunostaining (data not shown)

V. Supplementary References

1. Taylor RW, Barron MJ, Borthwick GM, et al. Mitochondrial DNA mutations in human colonic crypt stem cells. J Clin Invest 2003;112:1351-60.
2. Ramos A, Santos C, Alvarez L, et al. Human mitochondrial DNA complete amplification and sequencing: a new validated primer set that prevents nuclear DNA sequences of mitochondrial origin co-amplification. Electrophoresis 2009;30:1587-93.
3. Walther DJ, Peter JU, Bashammakh S, et al. Synthesis of serotonin by a second tryptophan hydroxylase isoform. Science 2003;299:76.
4. Engelstoft MS, Egerod KL, Lund ML, et al. Enteroendocrine cell types revisited. Curr Opin Pharmacol 2013;13:912-21.
5. Lembeck F. [The detection of 5-hydroxytryptamine in carcinoid metastases]. Naunyn Schmiedebergs Arch Exp Pathol Pharmakol 1954;222:235.
6. Lechago J. Neuroendocrine cells of the gut and their disorders. Monogr Pathol 1990:181-219.
7. Cunningham JL, Janson ET. The biological hallmarks of ileal carcinoids. Eur J Clin Invest 2011;41:1353-60.
8. Nilsson O. Profiling of ileal carcinoids. Neuroendocrinology 2013;97:7-18.
9. Trbojevic-Stankovic JB, Milicevic NM, Milosevic DP, et al. Morphometric study of healthy jejunal and ileal mucosa in adult and aged subjects. Histol Histopathol 2010;25:153-8.
10. Tomasetti C, Vogelstein B. Cancer etiology. Variation in cancer risk among tissues can be explained by the number of stem cell divisions. Science 2015;347:78-81.
11. Totafurno J, Bjerknes M, Cheng H. The crypt cycle. Crypt and villus production in the adult intestinal epithelium. Biophys J 1987;52:279-94.
12. Greaves LC, Preston SL, Tadrous PJ, et al. Mitochondrial DNA mutations are established in human colonic stem cells, and mutated clones expand by crypt fission. Proc Natl Acad Sci U S A 2006;103:714-9.
13. Baker AM, Cereser B, Melton S, et al. Quantification of crypt and stem cell evolution in the normal and neoplastic human colon. Cell Rep 2014;8:940-7.
14. Cheng H, Bjerknes M, Amar J, et al. Crypt production in normal and diseased human colonic epithelium. Anat Rec 1986;216:44-8.
15. Sei Y, Lu X, Liou A, et al. A stem cell marker-expressing subset of enteroendocrine cells resides at the crypt base in the small intestine. Am J Physiol Gastrointest Liver Physiol 2011;300:G345-56.